Biomaterials 283 (2022) 121437

Contents lists available at ScienceDirect

Biomaterials

journal homepage: www.elsevier.com/locate/biomaterials

Superoxide dismutase-loaded porous polymersomes as highly efficient antioxidant nanoparticles targeting synovium for osteoarthritis therapy

Tao Gui [a,b,1], Lijun Luo [c,d,1], Bonirath Chhay [c], Leilei Zhong [a], Yulong Wei [a,c], Lutian Yao [a], Wei Yu [a], Jun Li [a], Charles L. Nelson [a], Andrew Tsourkas [c], Ling Qin [a,**], Zhiliang Cheng [c,*]

[a] Department of Orthopaedic Surgery, University of Pennsylvania, Philadelphia, PA, 19104, USA
[b] Center for Joint Surgery and Sports Medicine, The First Affiliated Hospital, Jinan University, Guangzhou, China
[c] Department of Bioengineering, University of Pennsylvania, Philadelphia, PA, 19104, USA
[d] School of Agricultural Engineering, Jiangsu University, Jiangsu, China

ARTICLE INFO

Keywords:
Porous polymersomes
Antioxidant nanoparticles
Superoxide dismutase
Synovium
Osteoarthritis

ABSTRACT

Oxidative stress and the reactive oxygen species (ROS) have important roles in osteoarthritis (OA) development and progression. Scavenging ROS by exogenous antioxidant enzymes could be a promising approach for OA treatment. However, the direct use of antioxidant enzymes, such as superoxide dismutase (SOD), is challenging due to a lack of effective drug delivery system to knee joints. This study utilized a highly efficient antioxidative nanoparticle based on SOD-loaded porous polymersome nanoparticles (SOD-NPs) for delivery of SOD to mouse knee joints. The resultant SOD-NPs had prolonged mouse joint retention time with predominant accumulation in synovium but not in articular cartilage. Examining human synovial explants revealed that SOD-NPs minimize oxidative damages induced by OA-like insults. Intra-articular injections of SOD-NPs in mice receiving OA surgery were effective in attenuating OA initiation and preventing its further progression. Mechanistically, SOD-NPs reduced ROS production and the synthesis of catabolic proteases in both articular cartilage and synovium. Hence, our work demonstrates the therapeutic potential of SOD-NPs and indicate that targeting synovium holds a great promise for OA therapy.

1. Introduction

Knee osteoarthritis (OA) is a painful and debilitating musculoskeletal disease that can result in chronic joint pain, loss of joint function, and deleterious effects on the quality of daily life [1]. Current treatments for OA include non-pharmacological management, pharmacological treatments, and surgical approaches [2,3]. Although many pharmacologic treatments have been explored, there are no disease-modifying therapies available to delay OA progression or reverse the course of disease [4]. In most cases, pharmacological treatments are only palliative and accompanied by adverse side effects. Due to a lack of effective treatment approaches, over 600,000 knee replacements are performed each year in the US [5]. Currently, most drug studies aim to directly target articular cartilage for restoration of its integrity. Since OA is a whole joint disease, it is important to explore whether targeting other joint tissues, such as synovium, could be an effective OA treatment.

Previous studies demonstrated the critical role of oxidative stress and reactive oxygen species (ROS) in OA via regulating matrix metalloproteinase (MMP) production, chondrocyte apoptosis and senescence, extracellular matrix synthesis and degradation [6–10]. Under the healthy condition, ROS are produced at low levels in joint tissues. The adverse effects of ROS are normally blocked by the body's natural antioxidant defense system, including enzymatic and nonenzymatic antioxidants [11]. However, under the OA pathological condition, the balance between antioxidants and ROS is disrupted due to depletion of antioxidants, excess accumulation of ROS, or both, in cartilage and synovium [6]. This imbalance of cellular redox results in oxidative stress and damage in chondrocytes, leading to cartilage degradation.

Among multiple types of endogenous and exogenous antioxidants, such as phytochemicals, vitamins, and enzymes [12], superoxide dismutase (SOD), is the major catalytic antioxidant in joint tissues [13,14]. SOD catalyzes the conversion of superoxide radical ($O_2^{\bullet -}$) to hydrogen

* Corresponding author.
** Corresponding author.
E-mail addresses: qinling@pennmedicine.upenn.edu (L. Qin), zcheng@seas.upenn.edu (Z. Cheng).
[1] These authors contributed equally to this work.

https://doi.org/10.1016/j.biomaterials.2022.121437
Received 19 October 2021; Received in revised form 4 February 2022; Accepted 20 February 2022
Available online 23 February 2022

peroxide (H_2O_2). Previous studies showed that SOD activity is significantly decreased in OA joint tissues [15–17]. Several pilot trials have been performed by intra-articular injection of SOD into knee joint of patients suffering from active OA [18,19]. Thus, scavenging ROS by exogenous SOD could be a potential therapeutic strategy for OA treatment. However, the results of animal and clinical studies indicate that the direct use of free SOD only afford modest protective effect against oxidative damage due to intrinsic properties of SOD, namely, inadequate retention at the disease site and rapid inactivation of native SOD [20]. Therefore, developing an effective delivery system that improves SOD joint retention and protects against degradation could represent a new direction for OA therapy.

Nanomedicine is increasingly being used to improve therapeutic delivery for OA treatment due to the favorable pharmacokinetics, biodistribution, and solubility of nanoparticles (NPs) compared with free drugs [21–24]. Many NPs have recently been explored as carriers for SOD, including liposomes [25], poly(lactide-co-glycolide) (PLGA) [26], hollow silica nanospheres [27], polymersomes [28], and nanotubes/nanosheets [29,30]. However, most of these NPs possess notable limitations in terms of SOD delivery. For example, encapsulated SOD within liposomes exhibit improved protection against degradation, but suffers from loss of enzyme function and accessibility to ROS due to the absence of particle permeability [31]. PLGA-based NP systems are often associated with a poor drug loading for hydrophilic drugs, high burst release, and difficulties for surface functionalization [32,33]. Rapid enzyme inactivation remains a problem when SOD is conjugated or immobilized onto the surface of nanocarriers.

Polymersomes are a class of vesicles made from amphiphilic synthetic block copolymers that exhibit improved stability and a long *in vivo* retention time compared with phospholipid liposomes [34,35]. In order for antioxidant enzyme-loaded polymersomes to be used as an efficient NP-based antioxidant, they should allow ROS, *e.g.*, $O_2^{\bullet -}$, to pass into the aqueous interior and interact with encapsulated enzyme. Unfortunately, most polymersomes have a low intrinsic membrane permeability [34]. To overcome this challenge, we developed porous polymersomes with improved membrane permeability for small molecules [36,37]. By loading SOD into porous polymersomes, these SOD-NPs have showed beneficial effects in treating neurologic injury and myocardial ischemic reperfusion injury [36,37]. In this study, these constructs were characterized for their behavior in joint tissues and investigated for their effects in preventing and rescuing OA using a small animal model. To our surprise, we found that SOD-NPs mainly target synovium, but not articular cartilage, to achieve their therapeutic actions.

2. Materials and methods

2.1. Materials

Poly(ethylene glycol) (900)-polybutadiene (1800) copolymer (denoted PEG-PBD, MW 2700 Da) and Poly(ethylene glycol) (450)-poly (propylene oxide) (1400) (denoted PEG-PPO, MW 1850 Da) were purchased from Polymer Source (Dorval, Quebec, Canada). 1,2-dioleoyl-*sn*-glycero-3-phosphoethanolamine-N-(Lissamine rhodamine B sulfonyl) (Rhod-PE) was purchased from Avanti Polar Lipids, Inc. Cu/Zn Superoxide dismutase (SOD; MW 32500) from bovine erythrocytes was from Calbiochem (EMD Millipore, Billerica, MA). Fluorescein isothiocyanate (FITC) was purchased from Thermo Fisher Scientific. IRDye 800CW NHS Ester was purchased from LI-COR, Inc. All other chemicals were used as received. All of the buffer solutions were prepared with deionized water.

2.2. Synthesis of fluorescent labeled SOD

FITC-labeled SOD (FITC-SOD) was synthesized utilizing a molar ratio of 1/20 of SOD/FITC. Specifically, 1 mL 9.5 mg/mL SOD (in 10 mM PBS, pH 7.4)) was mixed with 455.31 μL 12.84 mM FITC (in anhydrous DMSO). After shaking at room temperature for 2 h, unconjugated FITC was removed by PD-10 column.

IRDye 800CW-labeled SOD (IRDye 800CW-SOD) was synthesized using a molar ratio of 1/10 of SOD/IRDye 800CW NHS Ester. Specifically, 1 mL 9.5 mg/mL SOD (in 10 mM PBS) was mixed with 58.5 μL 10 mM IRDye 800CW NHS Ester (in anhydrous DMSO). After shaking at room temperature for 2 h, unconjugated IRDye 800CW was removed by PD-10 column.

2.3. Synthesis and characterization of SOD-loaded nanoparticles

Briefly, stock solutions of PEG-PBD and PEG-PPO in chloroform were mixed in the following molar ratios: PEG-PBD/PEG-PPO (75:25). The total amount of PEG-PBD for each of the polymersome compositions was 20 mg. The solvent was removed using a direct stream of nitrogen prior to vacuum desiccation for at least 4 h 1 mL of 10 mg/mL SOD in 10 mM PBS (pH 7.4) was added to dried polymer films. Subsequently, the samples were incubated in a 55 °C water bath for 10 min and then sonicated for another 5 min. Samples were subjected to 5 freeze-thaw cycles in liquid nitrogen and warm H_2O (55 °C), followed by extrusion for at least 11 times through two stacked 200 nm Nuclepore polycarbonate filters using a mini extruder (Avanti Polar Lipids). After that, the sample was purified to remove nonentrapped SOD by centrifugal filter devices (Amicon Ultra-4, 100,000 MWCO, Millipore Corp.).

To prepare dual fluorescent dyes-labeled nanoparticles, 1 mL of 9.5 mg/mL FITC-SOD or IRDye 800CW-SOD was added to the dried polymer doped with 5 mol% Rhod-PE and freeze-thaw and extrusion were performed as described above. The nonentrapped FITC-SOD or IRDye 800CW-SOD was removed via size exclusion chromatography using Sepharose CL-4B (Sigma-Aldrich) and rehydration buffer as the eluent.

The measurement of SOD activity using the cytochrome *c* assay has been detailed previously [36,38]. The diameter and size distribution of nanoparticles were measured with dynamic light scattering (DLS, Malvern, Zetasizer, Nano-ZS). Ultraviolet–visible spectra (UV–Vis) and fluorescence spectra measurements were made on a Cary100 spectrophotometer (Varian) and a SPEX FluoroMax-3 spectrofluorometer (Horiba Jobin Yvon).

For stability assay, SOD-NPs were stored in 10 mM PBS (pH 7.4) at 4 °C. Measurement of nanoparticle structural integrity was acquired by monitoring the hydrodynamic diameter over the course of one week by dynamic light scattering (DLS). In addition, *in vitro* stability of SOD-NPs was also measured by DLS in 50% bovine synovial fluid (Vendors, Lampire biological laboratories, Inc.) at 37 °C for 24 h. The stability of SOD-NPs was tested in triplicate.

2.4. Cell culture

Primary mouse chondrocytes were isolated from the distal femoral of P3 (3 days after birth) C57Bl/6 mice as described previously with minor modification [39]. Briefly, cartilage tissues were incubated with 0.25% trypsin-EDTA (Invitrogen) for 30 min, followed by 600 U/mL type I collagenase (Worthington Biochemical) for 2 h. Primary mouse synovial fibroblasts (SFs) were isolated from joints of 2-month-old C57Bl/6 mice as described previously with minor modification [40]. Briefly, after euthanasia, mouse knee joints were harvested and washed with ice-cold PBS. The joint capsule was opened by reversing the quadricep to dissect synovial tissues out under the microscopy. Synovial tissues were first digested with 0.25% trypsin-EDTA for 30 min, followed by 300 U/mL type I collagenase digestion for 30 min. After filtered through a 70 μm strainer (Fisher Scientific), primary chondrocytes or SFs cells were cultured in growth medium (DMEM/F12 with 10% FBS, 100 μg/mL streptomycin, and 100 U/mL penicillin) to confluency.

For cell viability study, primary chondrocytes were seeded in 96-well plates at 5000 cells/well overnight, followed by SOD-NPs treatment (15.625–500 U/mL) for 24 h. 3-(4,5-dimethylthiazol-2-yl)-5-(3-carboxymethoxyphenyl)-2-(4-sulfophenyl)-2H-tetrazolium) (MTS) cell proliferation assay (Thermo Fisher Scientific) was then performed on these

cells. The absorbance of formazan product was measured on a Tecan microplate reader (BioTek Instruments, Inc.) at 490 nm. Cell viability was calculated using the following equation:

$$\text{Cell viability } (\%) = \text{Absorbance sample}/(\text{Absorbance control}) \times 100$$

For uptake assay, SFs were seeded in 24-well plate for 24 h at 5000 cells/well and then treated with SOD(FITC)-NP(Rhod) for another 24 h at 37 °C and 5% CO_2. The final FITC concentration in the culture medium was 10 μM. Cells were mounted with DAPI Fluoromount-G Mounting Medium (Southern Biotech) and observed under confocal microscope (Zeiss LSM 710). For intracellular ROS detection, SFs were treated with PBS, tumor necrosis factor-alpha (TNFα, 10 ng/mL, GenScript) in combination with PBS, free SOD (500 U/mL), SOD-NPs (500 U/mL) or a comparable dose of empty NPs for 24 h, followed by 10 μM 2′,7′-Dichlorodihydrofluorescein diacetate (H2DCFDA, MedChemExpress HY-D0940) in the dark for 30 min at 37 °C. Cells were detached from the dish by 0.05% trypsin-EDTA and immediately analyzed by flow cytometer (BD Biosciences, LSR II).

2.5. Human cartilage explant penetration assay

Human cartilage tissues were prepared from the de-identified specimens obtained at the total arthroplasty of the knee joints. Cartilage explants (6 mm in diameter and 3 mm in thickness) were harvested from lateral femoral condyle and cultured in chemically defined medium (DMEM, 1% ITS + Premix, 50 μg/mL L-proline, 0.1 μM dexamethasone, 0.9 mM sodium pyruvate and 50 μg/mL ascorbate 2-phosphate). They were treated with SOD-NP(Rhod-PE) for 0 (*i.e.*, preincubation), 2, 4, 6 and 8 days, respectively. Medium was replaced once every 2 days with SOD-NP(Rhod-PE). After incubation, cartilage explants were washed three times with PBS, fixed with 4% paraformaldehyde (PFA), dehydrated with 20% sucrose + 2% PVP (polyvinylpyrrolidone), followed by embedding with 20% sucrose + 2% PVP + 8% gelatin. Sections were mounted with DAPI Fluoromount-G Mounting Medium (Southern Biotech) and observed under confocal microscope (Zeiss LSM 710).

2.6. Human synovial explant experiments

Human synovial tissues were prepared from the de-identified specimens obtained at the total arthroplasty of the knee joints. They were cut into 5 mm (length) × 5 mm (width) × 2 mm (depth) explants with scissor and cultured in DMEM supplemented with 10% FBS, 1% ITS + Premix, 50 μg/mL L-proline, 1% Insulin, 100 μg/mL streptomycin, and 100 U/mL penicillin. Synovial explants were treated with PBS, interleukin-1β (IL-1β) in combination with PBS, free SOD, SOD-NPs or a comparable dose of empty NPs for 8 days. The final IL-1β and SOD activity in the culture medium was 10 ng/mL and 500 U/mL, respectively. Medium was replaced every two days. Explants were processed into 6 μm thick paraffin sections for immunohistochemistry staining.

2.7. Animal care and OA surgery

All animal work performed in this study was approved by the Institutional Animal Care and Use Committee at the University of Pennsylvania. To induce mouse OA, 3-month-old C57BL/6 male mice were subjected to destabilization of the medial meniscus (DMM) surgery at right knees and sham surgery at left knees as described previously [39]. Briefly, in DMM surgery, the joint capsule was opened under anesthesia and the medial meniscotibial ligament was cut to destabilize the meniscus without damaging other tissues. In Sham surgery, the joint capsule was opened in the same fashion but without any further damage. To test the therapeutic effect of SOD-NPs, 10 μl PBS, free SOD (500 U/mL), SOD-NPs (500 U/mL) or a comparable dose of empty NPs was injected intra-articularly with a 30-gauge needle into mouse right knees. The first injection was performed immediately after surgery or 4 weeks after the surgery. Injections were then repeated once every 2 weeks until 12 weeks after the DMM surgery.

2.8. In vivo joint retention assay

The mouse knee joint retention assay was assessed by intra-articular injection of 10 μl of 10 μM IRDye 800CW-labeled SOD or 10 μM IRDye 800CW-labeled SOD-NPs in healthy (5-month-old) and OA (5-month-old, 2 months post DMM surgery) mouse knee joints. An IVIS Spectrum (PerkinElmer) was used to serially acquire fluorescence images within each joint over a period of 4 weeks. Using Living Image software, radiant efficiency within a fixed anatomical region of interest (ROI) was measured.

2.9. SOD-NPs joint distribution assay

SOD-NPs joint distribution assay was performed by intra-articular injection of 10 μl of 10 μM SOD(FITC) or SOD(FITC)-NP(Rhod) in healthy (3-month-old) and injured (3-month-old, 3 days post DMM surgery) mouse knee joints. The joints were harvested at 1, 3, 7 and 14 days later for *in vivo* joint distribution analysis. Joints harvested at day 0 without any injection were used as negative control.

2.10. Histology

After euthanasia, mouse knee joints and major organs (kidney, liver, lung, heart, brain and spleen) were harvested and fixed in 4% PFA overnight. Organs were processed for paraffin sections followed by hematoxylin and eosin (H&E) staining. The knee joints were either decalcified in 0.5 M EDTA (pH 7.4) for 3 weeks for paraffin sections or cryosections. To prepare cryosections, samples were dehydrated in 20% sucrose and 2% PVP (polyvinylpyrrolidone), followed by embedding with 20% sucrose + 2% PVP + 8% gelatin, then a series of 75 μm-thick sagittal cryosections were cut across the joint.

For OA measurement, a serial of 6 μm-thick sagittal paraffin sections were cut across the entire medial compartment of the joint. Uncalcified cartilage area was defined from articular surface to tide mark. OA severity was measured by Mankin score as described previously [35]. Briefly, two sections within every consecutive six sections were stained with Safranin O/Fast green and scored by two blinded observers. For synovitis score, the following basic morphological parameters of synovitis were included [41]: (i) hyperplasia/enlargement of synovial lining layer, (ii) degree of inflammatory infiltration and (iii) activation of resident cells/synovial stroma, including fibroblasts, endothelial cells, histiocytes, macrophages, and multinucleated giant cells. All parameters are graded from 0 (absent), 1 (slight), 2 (moderate) to 3 (strong positive).

For immunohistochemistry assay, paraffin sections were incubated with primary rabbit antibodies against 8-hydroxy-2' -deoxyguanosine (8-OHdG, 1:100, bs-1278, Bioss), type II Collagen (1:50, ab34712, Abcam), Mmp13 (1:100, ab219620, Abcam), and Adamts5 (1:100, ab41037, Abcam) at 4 °C overnight, followed by binding with biotinylated secondary antibodies and DAB color development. Images were captured under a light microscope (Eclipse 90i, Nikon) and analyzed by Image J.

For immunofluorescence, cryosections were stained with primary antibody against mouse Pdgfrα (1:100, Santa Cruz Bio) at 4 °C overnight, followed by incubation with secondary antibody donkey anti-mouse Alexa 647(1:100, ab150107, Abcam) for 2 h at room temperature. The sections were then mounted with DAPI Fluoromount-G Mounting Medium and observed under confocal microscope (Zeiss LSM 710).

2.11. Micro-computed tomography (microCT) analysis

12 weeks after DMM surgery, mouse knee joints were harvested and the distal femur was scanned at a 6-μm isotropic voxel size with a

microCT 35 scanner (Scanco Medical AG, Brüttisellen, Switzerland). All images were smoothened by a Gaussian filter (sigma = 1.2, support = 2.0). To measure the subchondral bone plate (SBP) thickness as described previously [42], sagittal images were contoured for the SBP followed by generating a 3D color map of thickness for the entire SBP along with a scale bar. This map was then converted to a grayscale thickness map. The region of interest (ROI) was circled and the average SBP thickness within ROI was calculated.

2.12. OA pain analysis

The mouse knee joint pain was evaluated via von Frey filaments as described previously [39]. Individual mouse was placed on a wire-mesh platform (Excellent Technology Co.) under a 4 × 3 × 7 cm cage to restrict its movement. Mice were trained to be accustomed to this condition every day starting from 7 days before the test. During the test, a set of von Frey fibers (Stoelting Touch Test Sensory Evaluator Kit #2 to #9; ranging from 0.015 to 1.3 g force) were applied to the plantar surface of the hind paw until the fibers bowed, and then held for 3 s. The threshold force required to elicit withdrawal of the paw (median 50% withdrawal) was determined five times on each hind paw with sequential measurements separated by at least 5 min.

2.13. Statistical analysis

Data are expressed as means ± SEM and analyzed by t-tests, one-way analysis of variance (ANOVA) with Dunnett's or Turkey's post-test and or Turkey's post-test for multiple comparisons using Prism 8 software (GraphPad Software, San Diego, CA). Values of $p < 0.05$ were considered statistically significant.

3. Results and discussion

3.1. Characterization of SOD-NPs

Porous polymersomes with encapsulated SOD were prepared as antioxidant nanoparticles. Briefly, SOD was encapsulated within the aqueous interior of polymersomes made from a mixture of two amphiphilic diblock copolymers, 75 mol% poly(ethylene glycol)-polybutadiene copolymer (PEG-PBD) and 25 mol% poly(ethylene glycol)-poly(propylene oxide) (PEG-PPO) (Fig. 1A). The SOD encapsulation efficiency within these porous polymersomes was ~20%. The average diameter of the SOD-loaded polymersomes following freeze-thaw and extrusion was approximately 120 nm and low polydispersity (PDI, 0.2). The zeta potential of these nanoparticles in 10 mM Hepes buffer (pH 7.4) was −9.6 mV. To confirm that SOD was retained within the PEG-PPO-doped polymersomes, IRDye 800CW-labeled SOD was encapsulated into the polymersomes and then incubated in phosphate buffered saline (PBS) buffer for 24 h. Following centrifugation on a 100 K MWCO centrifugal filtering device, no fluorescence was detected in the flow-through, suggesting that the SOD is retained within the PEG-PPO-doped polymersomes (Fig. 1B). In contrast, nearly all encapsulated sulforhodamine B (SRB, 559 Da), a small fluorescent dye, was released within 24 h from the PEG-PPO-doped polymersomes (Figure S1A, Supporting Information). These findings clearly indicated that the PEG-PPO-doped polymersomes have high membrane permeability to small molecules, but not large molecules such as SOD. Accordingly, the activity of SOD within the PEG-PPO-doped polymersomes was significantly higher than that of the non-doped polymersomes. As shown in Figure S1B (Supporting Information), SOD activity in porous polymersomes was equally effective before and after dissolution of the polymersomes, suggesting that there is no loss in SOD activity in the porous polymersomes due to high accessibility to free superoxide radicals. The stability of the polymersomes was further evaluated in bovine synovial fluid. There was no observable change in the

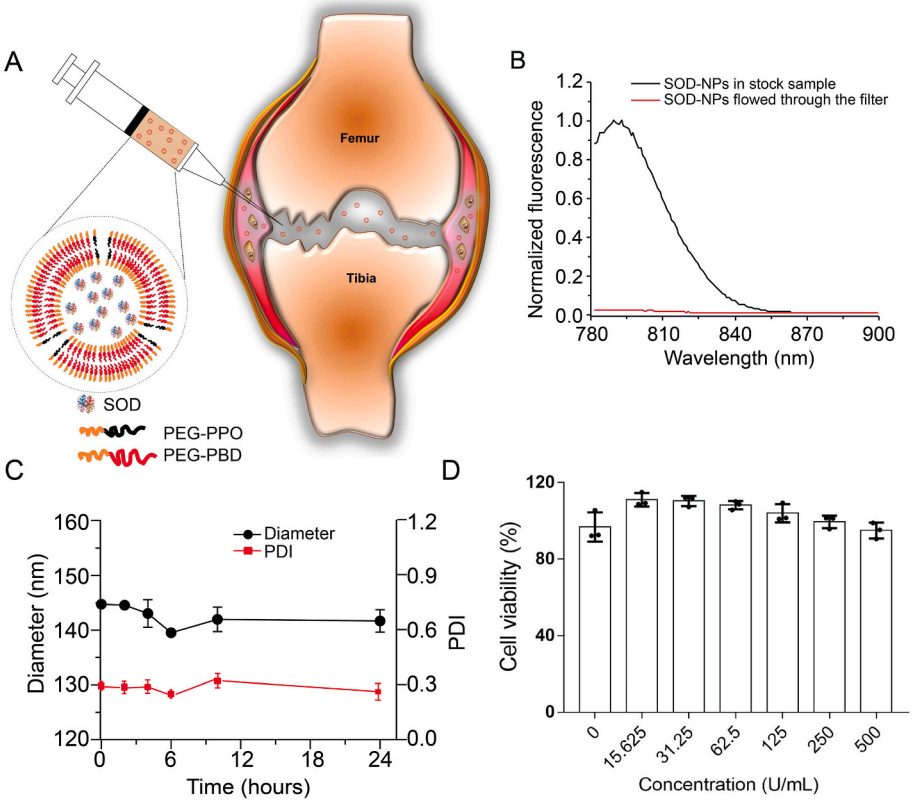

Fig. 1. Preparation and characterization of SOD-NPs. (A) Schematic diagram of SOD-loaded polymersomes with high membrane permeability for intra-articular joint injection. (B) Evaluation of SOD retention within PEG-PPO-doped polymersomes in PBS buffer (0.1 M, pH 7.4). The liquid that flowed through the filter was measured for fluorescence (red line). The fluorescence of unfiltered sample in the presence of Triton X-100 was also recorded (black line). The fluorescence intensity is normalized relative to the intensity of unfiltered sample at 790 nm. (C) The stability of SOD-NPs in bovine synovial fluid was accessed by monitoring the hydrodynamic diameter and PDI for up to 24 h. (D) The cytotoxicity of SOD-NPs was determined by measuring the cell viability of primary chondrocytes after coincubation with SOD-NPs at various SOD concentrations. (For interpretation of the references to color in this figure legend, the reader is referred to the Web version of this article.)

hydrodynamic diameter and polydispersity of polymersomes in bovine synovial fluid for 24 h (Fig. 1C). In addition, no significant SOD release from the PEG-PPO-doped polymersomes was observed following 24 h incubation in bovine synovial fluid (Figure S1C, Supporting Information). The cytotoxic effects of SOD-NPs were examined based on cell proliferation assay. In particular, various concentrations of SOD-NPs were incubated with primary mouse chondrocytes for 24 h. The cell viability for each group was normalized to a control group that was not incubated with any SOD-NPs. Generally, SOD-NPs had little effect on the viability of cells up to a SOD concentration of 500 U/mL (Fig. 1D).

3.2. SOD-NPs joint retention and biodistribution

To study the retention of SOD-NPs in the knee joints, SOD was labeled with IRDye 800CW and then encapsulated into PEG-PPO-doped porous polymersomes to obtain IRDye 800CW-SOD-NPs. Destabilization of the medial meniscus (DMM) surgery was performed on 3-month-old mice to induce knee OA. Two months later, sham or DMM-injured mice received a single injection of IRDye 800CW-SOD-NPs or IRDye 800CW-SOD to the knee joints. Fluorescence images of the knee joint region were acquired at various times after injection (Fig. 2A). Starting from day 5 under both normal and DMM conditions, SOD-NP-injected joints had much higher fluorescence intensity than those with free SOD injection. At day 28, fluorescence signal was still detectable in SOD-NP injected joints but not in joints injected with free SOD (Fig. 2B). Moreover, the retention of SOD-NPs in DMM joints was longer than that in healthy joints (Fig. 2C).

To further examine the *in vivo* biodistribution of SOD-NPs, we prepared dual fluorescent dye-labeled nanoparticles (SOD(FITC)-NP(Rhod)) by encapsulating FITC-SOD into Rhod-PE-doped polymersomes. A single intra-articular injection of SOD(FITC)-NP(Rhod) into mouse knees was performed. We first studied the biodistribution of NPs in DMM knees. In the absence of SOD-NPs (*i.e.*, day 0), no Rhod or FITC-based fluorescence signal was observed in any joint tissues including synovium and cartilage (Fig. 3A and B). However, injection of SOD (FITC)-NP(Rhod) led to a high, sustained fluorescence signal in the synovium over 14 days but almost no signal in the articular cartilage (Fig. 3B and C). As a control, a single injection of free SOD (FITC) into DMM-injured mouse knees resulted in a transient peak of FITC-based fluorescence signal in both synovium and articular cartilage at day 1–3 (Figure S2A,B, Supporting Information). Similar biodistribution results of SOD-NPs (Figure S3, Supporting Information) and free SOD (Figure S4, Supporting Information) were observed in healthy knee joints. Immunostaining of mouse joint at day 14 post SOD-NP injection revealed that most synovial cells with SOD-NP fluorescent signals are positive for platelet-derived growth factor receptor alpha (Pdgfrα), a fibroblast marker (Fig. 3D), indicating the uptake of SOD-NPs by synovial fibroblasts (SFs). These data demonstrate that compared to free SOD, SOD-NPs are predominantly accumulated in synovium with prolonged retention time.

To confirm that SOD-NPs cannot penetrate into cartilage, we incubated SOD-NP(Rhod) with human cartilage explants for 2, 4, 6, and 8 days. Confocal fluorescence images of cartilage section were acquired preincubation (day 0) and at various time points after incubation with SOD-NP(Rhod) (Figure S5, Supporting Information). Only a very weak fluorescence signal was observed within the top region of the articular cartilage, even up to 8 days. These results validate that the SOD-NPs are not able to penetrate into the articular cartilage, likely due to their relatively large size.

We also evaluated the biodistribution of SOD-NPs in other knee joint

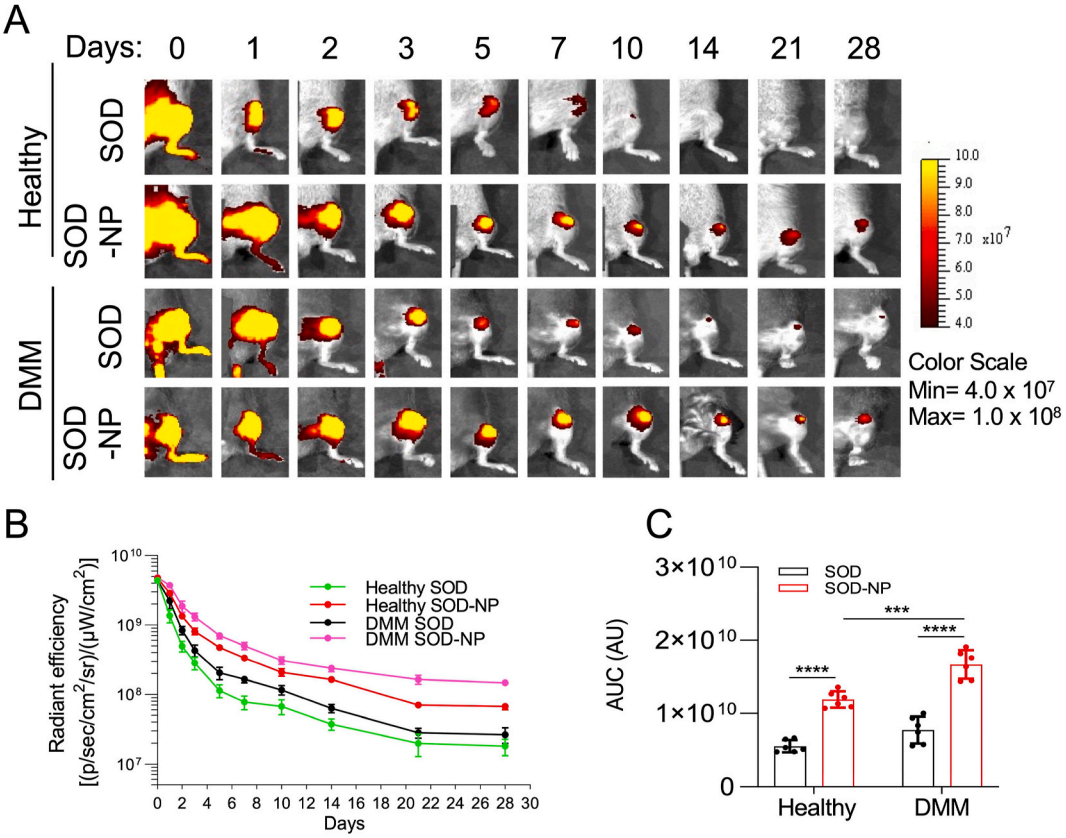

Fig. 2. Joint retention of SOD-NPs. (A) Representative images of healthy and OA mouse knee joints over 28 days after an intra-articular injection of IRDye 800CW–labeled SOD or SOD-NPs. (B) Quantitative analysis of time course radiant efficiency within knee joints after intra-articular injection of IRDye 800CW–labeled SOD or SOD-NPs. ($n = 6$ mice/group). (C) Quantitative analysis of area under the curve (AUC) based on fluorescence intensity profile in (B). ($n = 6$ mice/group). $^{***}P < 0.001$, $^{****}P < 0.0001$.

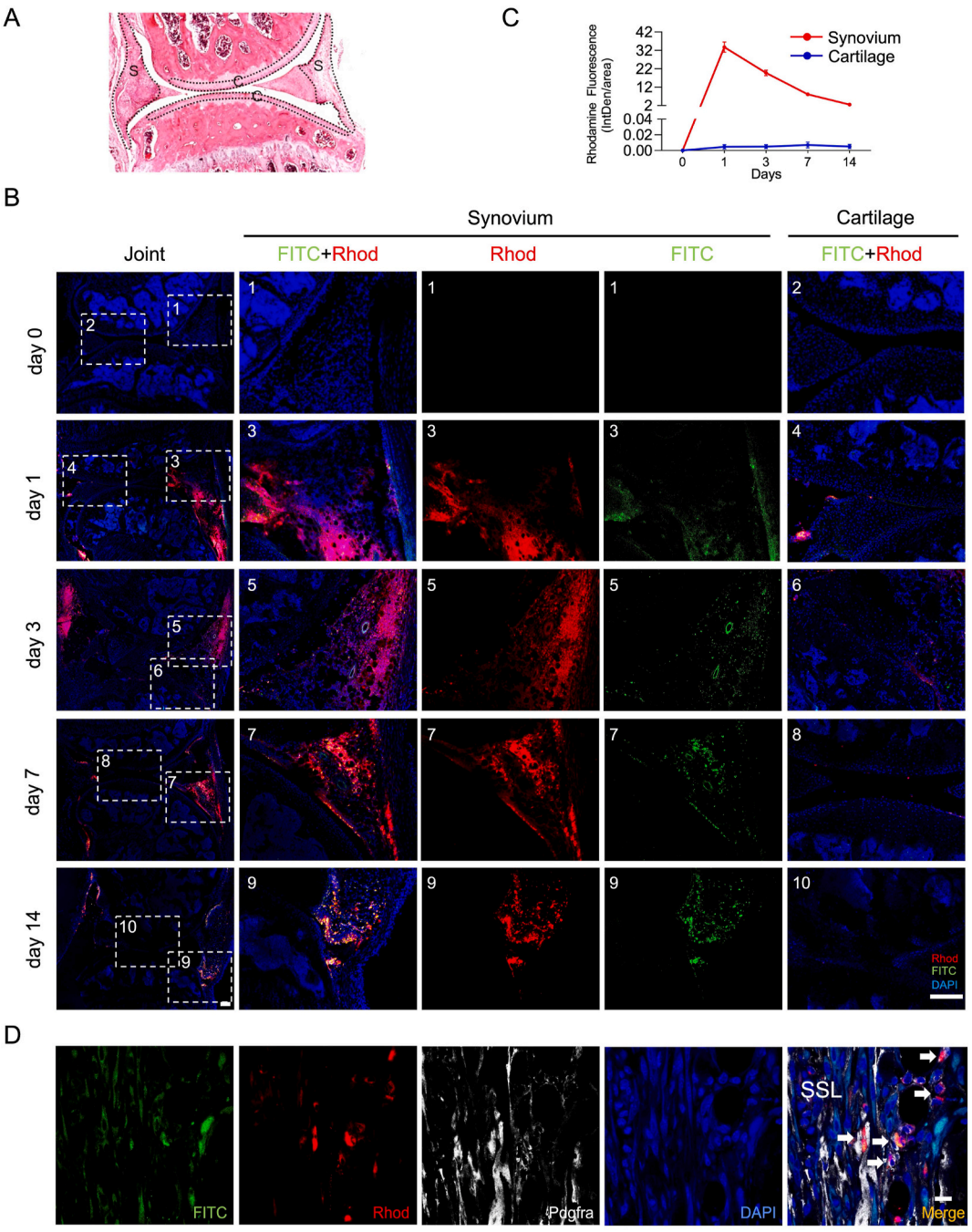

Fig. 3. *In vivo* biodistribution of SOD-NPs in DMM-injured mouse knee joint. (A) H&E staining of normal mouse knee joint showing the anatomy and location of synovium and cartilage. S: Synovium, C: Cartilage. (B) Representative fluorescence images of SOD(FITC)-NP(Rhod) distribution in mouse knee joints at day 0 (before injection) and 1, 3, 7 and 14 days after an intra-articular injection. Mice received DMM surgery two months before the injection. White boxes with the numbers in the joint images are magnified at the right to show synovium and cartilage. For synovial tissues, magnified regions labeled with FITC (green color), Rhod (red color) and the merged FITC, Rhod and DAPI (blue color) are provided, respectively. For cartilage tissues, only magnified regions from the merged FITC, Rhod and DAPI are provided. Scale bar: 200 μm. (C) Semi-quantification of rhodamine fluorescence intensity in synovium and cartilage. ($n = 3$ mice/group). (D) Immunofluorescence staining of Pdgfrα in mouse synovial tissue at 14 days post SOD(FITC)-NP(Rhod) injection. SSL: synovial sublining layer. Scale bar: 100 μm. (For interpretation of the references to color in this figure legend, the reader is referred to the Web version of this article.)

components, internal organs, and blood. At 24 h after a single intra-articular injection, fluorescence signals were detected on the surrounding soft tissues, including femoral condyles, tibial plateau and meniscus (Figure S6A,B, Supporting Information). The accumulation of the SOD-NPs was mainly observed in the liver and kidney, but no fluorescence signal was detected in blood, indicating that SOD-NPs were almost cleared from circulation (Figure S6C,D, Supporting Information). One month later, no fluorescence signal was observed in the liver and kidney.

3.3. SOD-NPs mitigate oxidative damages in OA synovial explants

Since *in vivo* biodistribution study suggested that SOP-NPs are mainly accumulated in synovium, we next investigated the effect of SOD-NPs on synovial cells. Adding SOD(FITC)-NP(Rhod) to cultured SFs clearly showed endocytosis of SOD-NPs (Fig. 4A). Flow cytometry revealed that

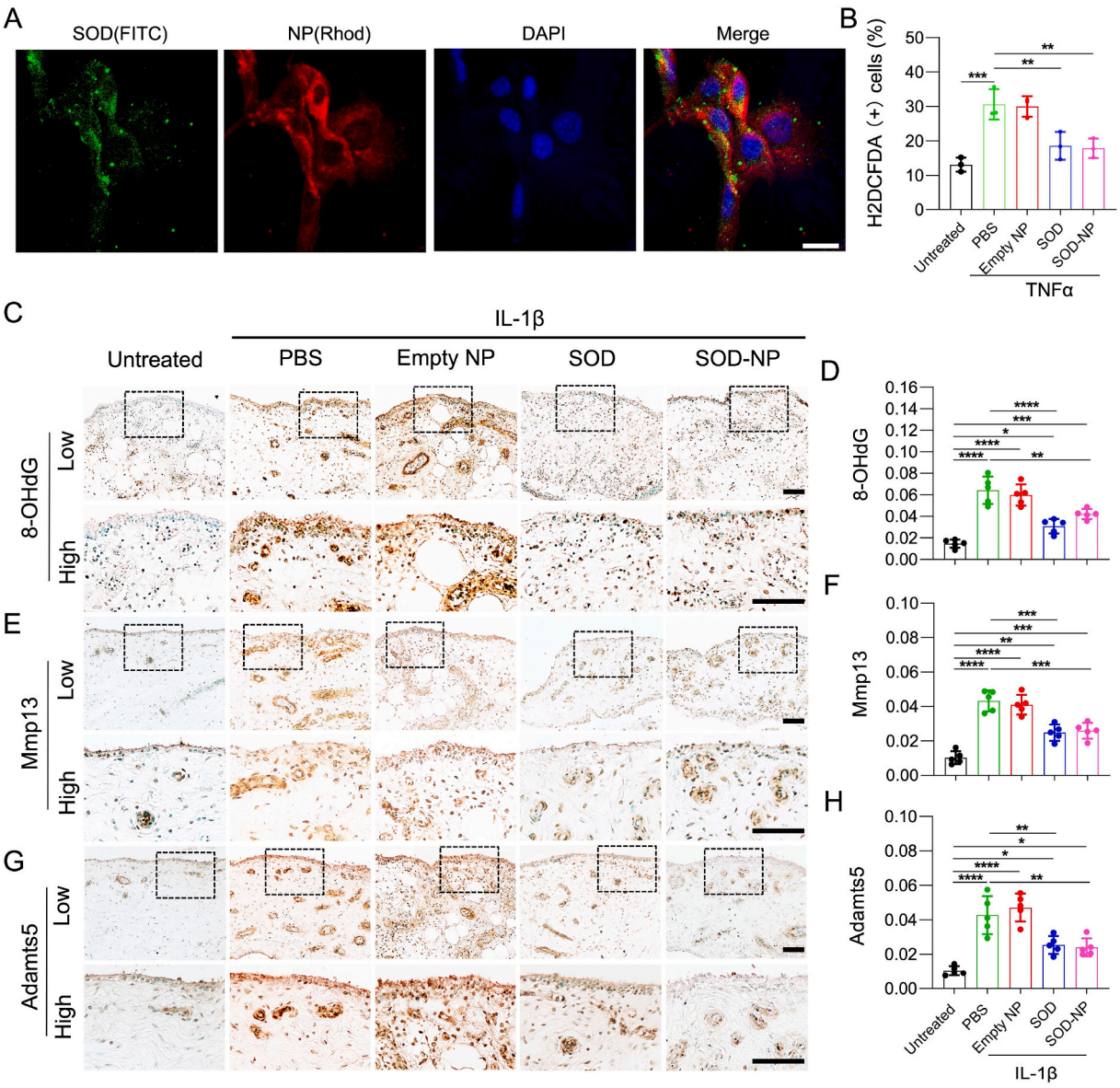

Fig. 4. Attenuation of oxidative damage by SOD-NPs in mouse SFs and human OA synovial explants. (A) Representative fluorescence images of mouse SFs treated with SOD(FITC)-NP(Rhod) for 24 h. Scale bar: 50 μm. (B) Measurement of H2DCFDA levels in mouse SFs after being treated by TNFα plus PBS, empty NP, SOD, or SOD-NP for 24 h. (C) Representative immunohistochemistry images of 8-OHdG in human synovial explants treated with PBS alone or IL-1β in combination with PBS, empty NP, SOD or SOD-NPs for 8 days. Scale bar: 100 μm. (D) The mean ratio of integrated optical density (IOD) to area (IOD/area) was used to semi-quantify 8-OHdG amount. (n = 5 explants/group). (E) Immunohistochemistry staining of Mmp13. Scale bar, 100 μm. (F) Semi-quantitative evaluation of Mmp13 amount represented as IOD/area. (n = 5 explants/group). (G) Immunohistochemistry staining of Adamts5. Scale bar: 100 μm. (H) Semi-quantitative evaluation of Adamts5 amount represented as IOD/area. (n = 5 explants/group). In panels C, E, and G, the bottom images are the magnified images from the squared regions from the top images. Low: low magnification; high: high magnification. *P < 0.05, **P < 0.01, ***P < 0.001, ****P < 0.0001.

TNFα drastically increased ROS level, marked by H2DCFDA, in SFs by 2.3-fold (Fig. 4B and Figure S7, Supporting Information). This increase was attenuated by SOD and SOD-NPs, but not empty NP (*i.e.*, no SOD encapsulation), suggesting potent anti-ROS activity of SOD-NPs. Next, we cultured human synovial explants and treated them with IL-1β to induce OA-like phenotypes. As expected, 8 days of IL-1β treatment drastically increased the amounts of oxidative stress marker 8-OHdG) by 4.4-fold, and catabolic proteases Mmp13 and Adamts5 by 4.2- and 4.1-fold, respectively, in both synovial lining layer and sublining layer (Fig. 4C–H). Empty NP alone did not affect these OA-related changes. Meanwhile, SOD addition significantly attenuated IL-1β-induced 8-OHdG, Mmp13, and Adamts5 amounts by 52.1%, 42.7%, and 40.5%, respectively. SOD-NPs had a similar effect, leading to 34.4%, 40.2%, and 43.8% reductions compared to IL-1β alone. We conclude that SOD-NPs are as potent as free SOD in blocking OA-induced oxidative damage *in vitro*.

3.4. SOD-NPs attenuate joint destruction in a surgery-induced mouse OA model

We next investigated the *in vivo* therapeutic effect of SOD-NPs. For this purpose, we performed DMM surgery on mouse knee joints to induce OA. SOD-NPs were then injected into knee joints once every two weeks for 12 weeks, starting immediately after the DMM surgery (Fig. 5A). Control groups included PBS, empty NP, and free SOD injections. At 12 weeks post DMM surgery, PBS- and empty NP-treated groups showed a similar level of cartilage degeneration (Fig. 5B). Specifically, a large portion of articular cartilage was eroded and cartilage

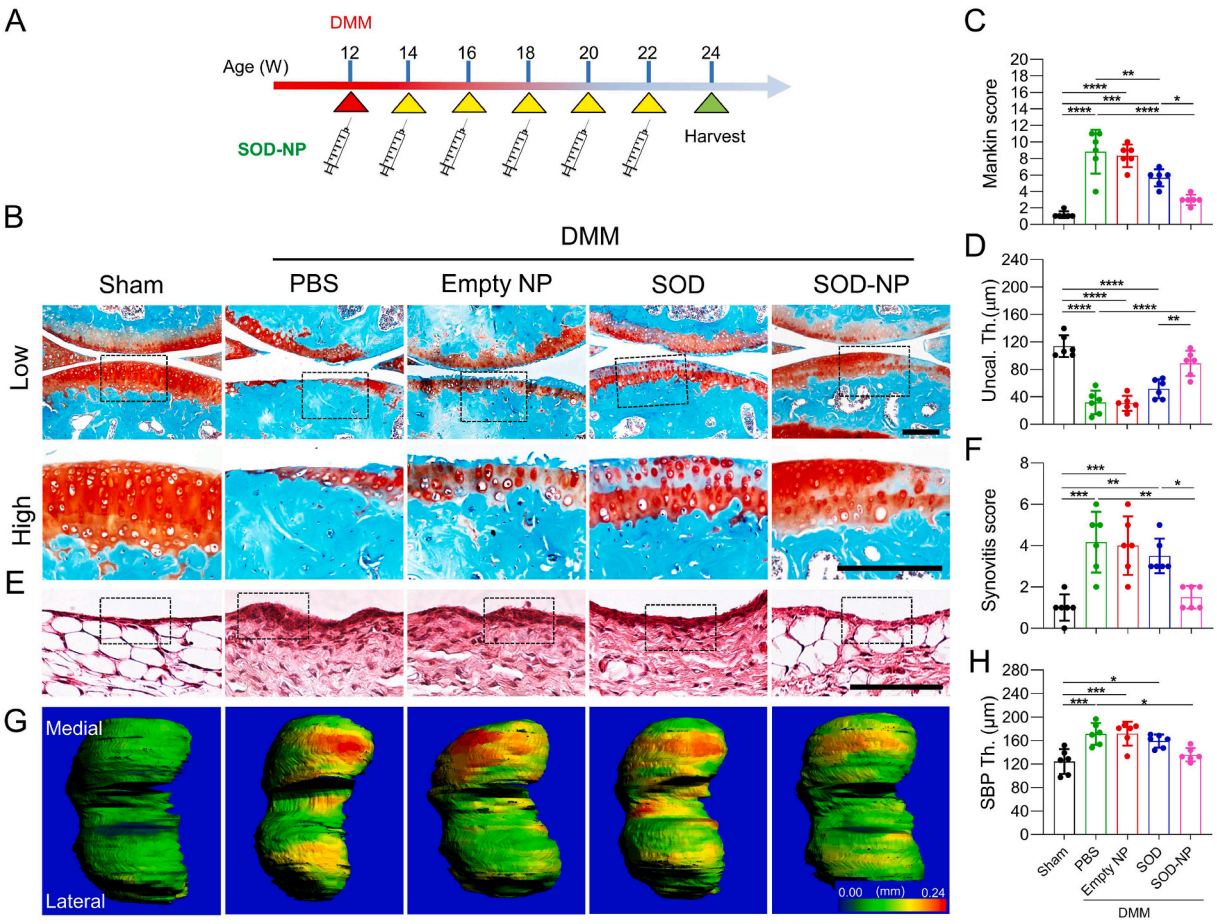

Fig. 5. Evaluation of the therapeutic efficacy of SOD-NP treatment starting immediately after the DMM surgery. (A) Schematic diagram of study design. WT mice at 12 weeks of age received sham or DMM surgery and were treated by intra-articular injections of PBS, empty NP, SOD or SOD-NPs immediately and once every 2 weeks afterwards. Joints were harvested 12 weeks later for analyses. (B) Safranin O/Fast Green staining of knee joints at 12 weeks after surgery. Low: low-magnification images; high: high-magnification images of black boxed areas above. Scale bars, 200 μm. (C) The OA severity of knee joints was measured by Mankin score. ($n = 6$ mice/group). (D) Average uncalcified cartilage thickness (Uncal. Th.) of knee joints. ($n = 6$ mice/group). (E) H&E staining of synovium. Black boxed areas indicate the synovial tissues. Scale bar, 200 μm. (F) Synovitis scores were quantified. ($n = 6$ mice/group). (G) Representative 3D color maps derived from micro-CT images showing femoral SBP thickness. Color ranges from 0 (blue) to 240 μm (red). (H) Quantification of SBP thickness. ($n = 6$ mice/group). $^*P < 0.05$, $^{**}P < 0.01$, $^{***}P < 0.001$, $^{****}P < 0.0001$. (For interpretation of the references to color in this figure legend, the reader is referred to the Web version of this article.)

surface fibrillation and cleft were obviously presented, leading to Mankin scores of 8.8 and 8.3 in PBS- and empty NP-treated groups, respectively (Fig. 5C). Interestingly, injections of free SOD alone partially attenuated this OA phenotype, with more cartilage remaining, compared to PBS and empty NP-treated groups. Meanwhile, injections of SOD-NPs maintained most cartilage integrity. The Mankin score of SOD-NP-treated group was significantly reduced compared to PBS-, empty NP-, and free SOD-treated groups. The uncalcified zones were also largely preserved in the SOD-NP-treated group (Fig. 5D), suggesting that SOD-NP treatment can efficiently attenuate OA development.

In addition to cartilage phenotypes, OA progression in DMM mice is also accompanied with synovitis and subchondral bone plate (SBP) sclerosis [43,44]. At 12 weeks post DMM surgery, synovium thickening is apparent in DMM mice with PBS and empty NP treatment, resulting in synovitis scores of 4.1 and 4.0 respectively (Fig. 5E and F). Free SOD alone did not affect this change. However, SOD-NPs treatment significantly reduced the synovitis score to 1.5, comparable to 1.0 in sham joints. Since DMM is performed at the medial site, SBP thickness at the medial site, but not at the lateral site, increased by 38.0% at 12 weeks post-surgery in PBS treated group (Fig. 5G and H). While this bone plate sclerosis persists in empty NP- and free SOD-treated groups, SOD-NP treatment partially mitigated this change.

To understand the mechanism of the therapeutic effect of SOD-NPs, we performed staining for an oxidative stress biomarker (8-OHdG), the major component of the cartilage matrix (collagen II), and extracellular matrix proteases including Mmp13 and Adamts5 in the joints. DMM drastically increased 8-OHdG, Mmp13, and Adamts5 staining in synovium (Fig. 6A–F) and articular cartilage (Fig. 6G-N). Both SOD and SOD-NPs treatment decreased the amounts of 8-OHdG, Mmp13 and Adamts5 in synovium, but the effect of SOD-NPs (48.9%, 55.2%, 42.8% decreases in 8-OHdG, Mmp13 and Adamts5 amounts, respectively, compared to PBS) was much more drastic than with free SOD alone (26.8%, 26.2%, and 19.5% decreases, respectively). While free SOD alone reduced 8-OHdG in the articular cartilage, it did not alter Mmp13, Adamts5, and collagen II amounts compared to PBS treatment. Meanwhile, SOD-NPs reduced the staining of 8-OHdG, Mmp13, Adamts5 and collagen II in the articular cartilage of DMM knees to the levels similar to those in sham knees.

We also examined whether SOD-NPs caused any side effects to overall joint structure and major internal organs. The gross morphology of knee joints was not altered by 12 weeks of SOD-NP treatment (Figure S8A, Supporting Information). We also did not observe any obvious morphologic changes in the heart, liver, spleen, lung, kidney or brain between sham groups and SOD-NP-treated groups (Figure S8B, Supporting Information).

Lastly, to mimic a clinical scenario, we allowed OA to develop for 4

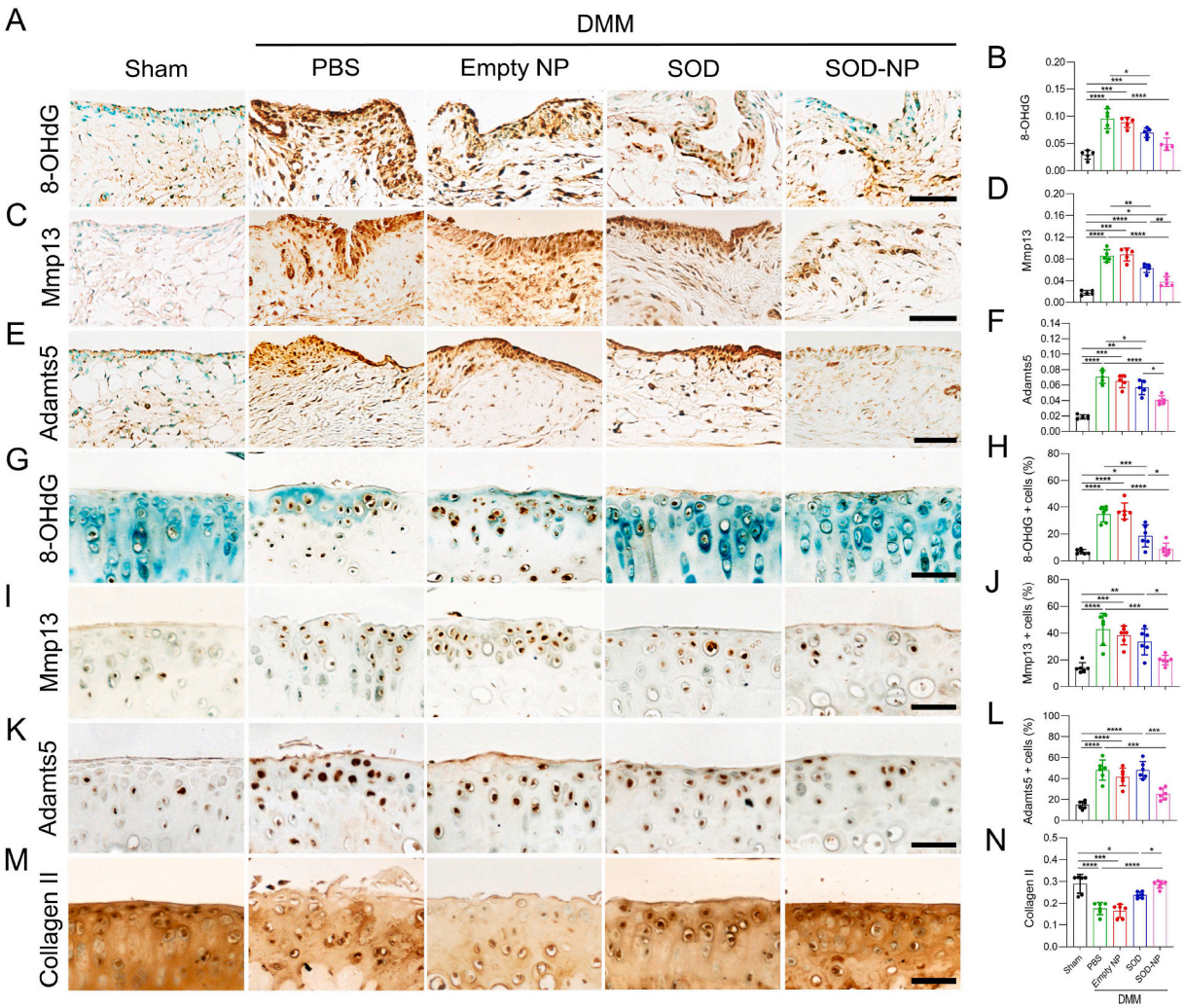

Fig. 6. Effects of SOD-NPs on oxidative stress and matrix degradation *in vivo*. WT mice at 12 weeks of age received sham or DMM surgery and were treated by intra-articular injections of PBS, empty NP, SOD or SOD-NPs immediately and once every 2 weeks afterwards. Joints were harvested 12 weeks later for immunohistochemistry. Representative staining images of ROS marker 8-OHdG (A, G), Mmp13 (C, I), Adamts5 (E, K) and collagen II (M) in synovium (A, C, E) and articular cartilage (G, I, K, M) are shown. Scale bar: 50 μm. The amounts of 8-OHdG, Mmp13, and Adamts5 in synovium were quantified in (B), (D), and (F), respectively. The percentages of chondrocytes positive for 8-OHdG, Mmp13, and Adamts5 in articular cartilage were quantified in (H), (J) and (L) respectively. Mean Optical Density of collagen II staining in articular cartilage was presented in (N). ($n = 6$ mice/group). $^{*}P < 0.05$, $^{**}P < 0.01$, $^{***}P < 0.001$, $^{****}P < 0.0001$.

weeks after DMM surgery and then treated mice with SOD-NPs and controls (Fig. 7A). Another 8 weeks later, we observed severe cartilage degeneration and synovitis in PBS-, empty NP- and free SOD-treated groups (Fig. 7B and C). Strikingly, SOD-NPs were capable of attenuating OA progression, as indicated by reduced Mankin score (Fig. 7D) and synovitis score (Fig. 7E) compared to control groups. Moreover, von Frey assay revealed that SOD-NP treatment attenuated OA-induced pain during the treatment period (Fig. 7F). Thus, our results demonstrate the therapeutic effects of SOD-NPs in preventing and rescuing OA development in a mouse model.

3.5. Discussion

Most current nanomedicine for OA therapy has focused on cartilage-targeting drug delivery. Generally, small nanoparticles penetrate cartilage more efficiently than large nanoparticles. Introducing an optimal positive charge to small NPs could further increase their transport and enable full thickness cartilage penetration. For example, Geiger et al. conjugated insulin-like growth factor 1 (IGF-1) onto positively-charged polyamidoamine (PAMAM) dendrimers (<10 nm) and showed that the dendrimer-IGF-1 conjugates penetrated full thickness cartilage within 2 days [21]. Similarly, Bajpayee et al. demonstrated that the highly positively charged Avidin (~7 nm, mimicking the small size NPs) penetrated into the full thickness of cartilage explants [45]. Our previous studies also revealed that positively charged phospholipid micelles (<15 nm) could penetrate into the full depth of cartilage [46]. To use these small-sized NPs as drug carriers for cartilage targeted OA treatment, small molecule drugs are often physically entrapped into NPs, and biological macromolecules like peptides and antibodies are often chemically conjugated onto NPs. However, the conjugation of SOD onto the surface of these NPs could not protect SOD from rapid degradation. To solve this challenge, an alternative approach is to entrap SOD within large, targeted NPs (>100 nm), so the NP layer provides a protective membrane for SOD against degradation. As described in the introduction, some large nanoparticles, such as liposomes, polymersomes and PLGA, have been used as nanocarriers for SOD loading. In this work, we used PEG-PPO-doped porous polymersomes for SOD encapsulation. The encapsulated SOD was surrounded by a highly permeable membrane, which prevents SOD degradation and allows full access of ROS, *e.g.*, $O_2^{\bullet -}$, to the SOD. In addition, an unobstructed outer surface of SOD-encapsulated porous polymersomes can be used for the highly efficient attachment of any other functional agents, including targeting

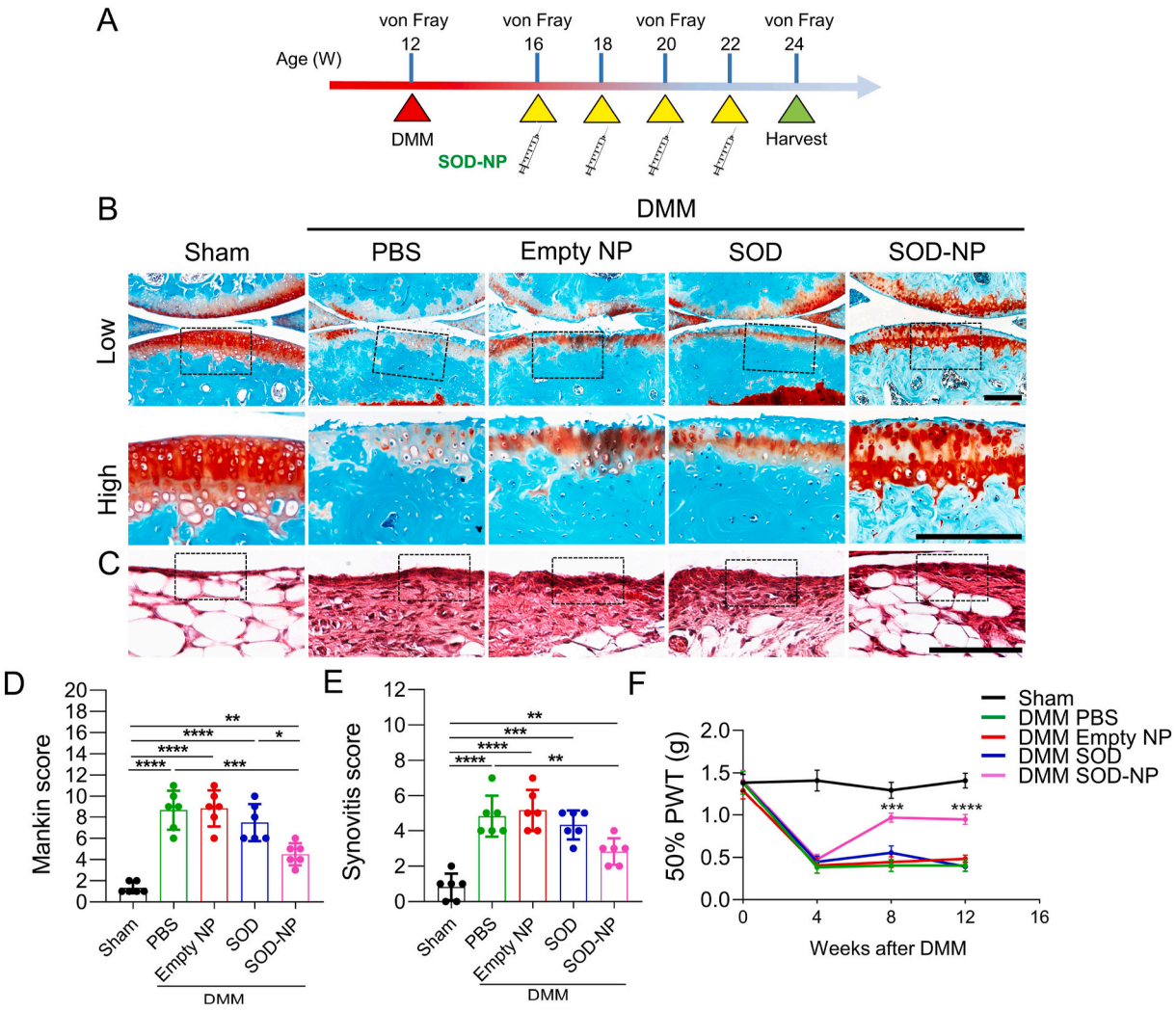

Fig. 7. Evaluation of therapeutic efficacy of SOD-NP treatment starting at 4 weeks after DMM surgery. (A) Schematic diagram of study design. WT mice at 12 weeks of age received sham or DMM surgery and were treated by intra-articular injections of PBS, empty NP, SOD or SOD-NPs starting at 4 weeks post-surgery with a frequency of once every 2 weeks. Joints were harvested 12 weeks after surgery for analyses. (B) Safranin O/Fast Green staining of knee joints. Low: low-magnification image; high: high-magnification image of the black boxed area above. Scale bars, 200 μm. (C) H&E staining of synovium. Black boxed areas indicate synovial tissue. Scale bar, 200 μm. (D) The OA severity of knee joints in (B) was measured by Mankin score. ($n = 6$ mice/group). (E) Synovitis score of (C) was measured. ($n = 6$ mice/group). (F) von Frey assay at 4, 8 and 12 weeks after DMM surgery. The data of day 0 was acquired before DMM surgery. PWT: paw withdrawal threshold. ($n = 6$ mice/group). $^{*}P < 0.05$, $^{**}P < 0.01$, $^{***}P < 0.001$, and $^{****}P < 0.0001$ in (D) and (E). $^{***}P < 0.001$ and $^{****}P < 0.0001$ for SOD-NP versus PBS in (F). (For interpretation of the references to color in this figure legend, the reader is referred to the Web version of this article.)

ligands or imaging contrast agents in the future.

In vivo biodistribution study in mice revealed that SOD-NPs were retained mostly in synovial tissue, but not in articular cartilage, after intra-articular injections. Since OA is recognized as a whole joint disease [47], synovial inflammation is an important risk factor in OA initiation and progression [44,48,49]. Synovium is a specialized connective tissue that forms the lining of bursae and fat pads to seal the synovial cavity and fluid from surround tissues [44]. It predominantly consists of fibroblast like synoviocytes that provide lubricating molecules, such as Proteoglycan 4 (Prg4) and hyaluronic acid, and plasma-derived nutrients to the joint cavity and the adjacent cartilage [50]. During OA progression, synovial tissue undergoes characteristic changes, such as synovial lining hyperplasia, sublining fibrosis, and stromal vascularization [51]. These changes are not only associated with OA pain but also likely provides catabolic signals to the articular cartilage [44]. Previous studies suggest that synovial inflammation may occur even before cartilage degeneration, with infiltration of mononuclear cells, thickening of the synovial lining layer and production of inflammatory cytokines [44]. Our studies clearly showed that inflammatory cytokines TNFα and IL-1β increase ROS level in SFs and synovial explants. Moreover, IL-1β stimulates the production of destructive proteinases Mmp13 and Adamts5 in synovial explants. Those secreted catabolic factors could in turn act on cartilage matrix to promote cartilage degradation. SOD-NPs can be endocytosed into SFs, leading to attenuated ROS reaction and proteinase production, as well as reduced synovitis symptoms and OA pain relief. Therefore, different from other studies that mainly targets cartilage for OA treatment, our SOD-NPs could offer another approach that targets synovium for OA therapy.

Due to technical challenges of collecting the synovial fluid from mouse knee joints, we did not analyze the ROS level in synovial fluid following SOD-NP treatment. However, it is reasonable to expect that SOD-NPs can also act as scavengers for ROS in the synovial fluid. In future large animal studies, synovial fluid can be collected at different times during the treatment.

Considering the future clinical translation of SOD-NPs, we have tested the therapeutic effects of SOD-NPs in human synovial explants. In addition, we also evaluated the ability of SOD-NPs to block OA progression at 4 weeks after DMM injury. This is important since in most

cases patients already display OA symptoms when they show up in the clinic. However, the current study has several limitations. For example, in this work, only SOD was encapsulated into the porous polymersomes. Co-loading other antioxidants, such as catalase, within the NPs could further minimize damage caused by other ROS, such as hydrogen peroxide (H_2O_2). We have used fluorescence imaging to study the penetration, retention and biodistribution of SOD-NPs within the tissues and joints. However, SOD labeled with fluorescent dyes could have different behaviors than native SOD. In future studies, a radiolabeling technique will be considered. While our current engineered SOD-NPs showed the therapeutic effects in a mouse OA model induced by DMM surgery, further studies are needed to validate the efficacy of these NPs in different OA models, such as spontaneous OA. Large animal models are also needed because the joint anatomy and physiology of small animals (*i.e.*, mice) are significantly different from large animals and humans. As noted above, OA is considered as a disease of the whole joint and inflammation could occur in other joint tissues, such as cartilage. Thus, nanoparticles targeting both synovium and cartilage could achieve a better therapeutic efficacy compared to the current formulation. In the future, we will explore this by adjusting some properties of nanoparticles including size, surface charge, surface chemistry and etc.

4. Conclusions

The therapeutic utility of the antioxidant enzyme SOD is largely hindered by inadequate delivery, stability, and retention at the intended site of action, due to rapid degradation and clearance. This is a critical problem for the efficient removal of ROS in OA joints. Our study demonstrates that SOD-loaded porous polymersomes are more efficacious than free SOD in treating OA by targeting synovium followed by cartilage protection.

Author contributions

Ling Qin and Zhiliang Cheng conceived idea and designed experiments. Tao Gui, Lijun Luo, Jun Li and Yulong Wei performed animal experiments. Lijun Luo and Bonirath Chhay made NP formulations. Tao Gui and Lutian Yao performed the histology and imaging analysis. Charles L Nelson provided human joint tissues and assisted histology analysis. Lijun Luo and Leilei Zhong performed cell culture and flow analysis. Tao Gui and Wei Yu performed micro-CT analysis. Ling Qin and Zhiliang Cheng wrote the manuscript. Andrew Tsourkas reviewed and revised the manuscript. Ling Qin and Zhiliang Cheng approved the final version.

Data availability

The data that supports this study is available from the authors upon reasonable request.

Declaration of competing interest

The authors declare that they have no known competing financial interests or personal relationships that could have appeared to influence the work reported in this paper.

Acknowledgements

This work was supported in part by the National Institutes of Health R01NS100892 (Z.C.), R01AG067698, R21AR078650 (to L.Q.), P30AR069619 (to Penn Center for Musculoskeletal Disorders), and the 2019 Health Research Formula Fund from the Pennsylvania Department of Health.

Supporting Information

Supporting Information is available from the Elsevier Online Library or from the author.

Appendix A. Supplementary data

Supplementary data to this article can be found online at https://doi.org/10.1016/j.biomaterials.2022.121437.

References

[1] T. Neogi, The epidemiology and impact of pain in osteoarthritis, Osteoarthritis Cartilage 21 (9) (2013) 1145–1153.
[2] L.F. Kou, S.Y. Xiao, R. Sun, S.H. Bao, Q. Yao, R.J. Chen, Biomaterial-engineered intra-articular drug delivery systems for osteoarthritis therapy, Drug Deliv. 26 (1) (2019) 870–885.
[3] K. Sinusas, Osteoarthritis: diagnosis and treatment, Am. Fam. Physician 85 (1) (2012) 49–56.
[4] M.A. Karsdal, M. Michaelis, C. Ladel, A.S. Siebuhr, A.R. Bihlet, J.R. Andersen, H. Guehring, C. Christiansen, A.C. Bay-Jensen, V.B. Kraus, Disease-modifying treatments for osteoarthritis (DMOADs) of the knee and hip: lessons learned from failures and opportunities for the future, Osteoarthritis Cartilage 24 (12) (2016) 2013–2021.
[5] L.A. MacFarlane, E. Kim, N.R. Cook, I.M. Lee, M.D. Iversen, J.N. Katz, K. H. Costenbader, Racial variation in total knee replacement in a diverse nationwide clinical trial, J. Clin. Rheumatol. 24 (1) (2018) 1–5.
[6] P. Lepetsos, A.G. Papavassiliou, ROS/oxidative stress signaling in osteoarthritis, Biochim. Biophys. Acta 1862 (4) (2016) 576–591.
[7] F.J. Blanco, R.L. Ochs, H. Schwarz, M. Lotz, Chondrocyte apoptosis induced by nitric-oxide, Am. J. Pathol. 146 (1) (1995) 75–85.
[8] A. Klamfeldt, S. Marklund, Enhanced breakdown in vitro of bovine articular cartilage proteoglycans by conditional synovial medium. The effect of superoxide dismutase and catalase, Scand. J. Rheumatol. 16 (1) (1987) 41–45.
[9] J.C. Monboisse, J.P. Borel, Oxidative damage to collagen, EXS 62 (1992) 323–327.
[10] H. Burkhardt, M. Schwingel, H. Menninger, H.W. Macartney, H. Tschesche, Oxygen radicals as effectors of cartilage destruction - direct degradative effect on matrix components and indirect action via activation of latent collagenase from polymorphonuclear leukocytes, Arthritis Rheum. 29 (3) (1986) 379–387.
[11] S.B. Nimse, D. Pal, Free radicals, natural antioxidants, and their reaction mechanisms, RSC Adv. 5 (35) (2015) 27986–28006.
[12] K. Rahman, Studies on free radicals, antioxidants, and co-factors, Clin. Interv. Aging 2 (2) (2007) 219–236.
[13] M. Koike, H. Nojiri, H. Kanazawa, H. Yamaguchi, K. Miyagawa, N. Nagura, S. Banno, Y. Iwase, H. Kurosawa, K. Kaneko, Superoxide dismutase activity is significantly lower in end-stage osteoarthritic cartilage than non-osteoarthritic cartilage, PLoS One 13 (9) (2018), e0203944.
[14] E.A. Regan, R.P. Bowler, J.D. Crapo, Joint fluid antioxidants are decreased in osteoarthritic joints compared to joints with macroscopically intact cartilage and subacute injury, Osteoarthritis Cartilage 16 (4) (2008) 515–521.
[15] J.L. Scott, C. Gabrielides, R.K. Davidson, T.E. Swingler, I.M. Clark, G.A. Wallis, R. P. Boot-Handford, T.B. Kirkwood, R.W. Taylor, D.A. Young, Superoxide dismutase downregulation in osteoarthritis progression and end-stage disease, Ann. Rheum. Dis. 69 (8) (2010) 1502–1510.
[16] E. Regan, J. Flannelly, R. Bowler, K. Tran, M. Nicks, B.D. Carbone, D. Glueck, H. Heijnen, R. Mason, J. Crapo, Extracellular superoxide dismutase and oxidant damage in osteoarthritis, Arthritis Rheum. 52 (11) (2005) 3479–3491.
[17] C. Ruiz-Romero, V. Calamia, J. Mateos, V. Carreira, M. Martinez-Gomariz, M. Fernandez, F.J. Blanco, Mitochondrial dysregulation of osteoarthritic human articular chondrocytes analyzed by proteomics: a decrease in mitochondrial superoxide dismutase points to a redox imbalance, Mol. Cell. Proteomics 8 (1) (2009) 172–189.
[18] K. Lund-Olesen, K.B. Menander, Orgotein: a new anti-inflammatory metalloprotein drug: preliminary evaluation of clinical efficacy and safety in degenerative joint disease, Curr. Ther. Res. Clin. Exp. 16 (7) (1974) 706–717.
[19] L. Flohé, Superoxide dismutase for therapeutic use: clinical experience, dead ends and hopes, Mol. Cell. Biochem. 84 (2) (1988) 123–131.
[20] X. Gao, Y.Q. Ma, G.J. Zhang, F.Y. Tang, J.J. Zhang, J.C. Cao, C.H. Liu, Targeted elimination of intracellular reactive oxygen species using nanoparticle-like chitosan- superoxide dismutase conjugate for treatment of monoiodoacetate-induced osteoarthritis, Int. J. Pharm. 590 (2020) 119947.
[21] B.C. Geiger, S. Wang, R.F. Padera, A.J. Grodzinsky, P.T. Hammond, Cartilage-penetrating nanocarriers improve delivery and efficacy of growth factor treatment of osteoarthritis, Sci. Transl. Med. 10 (469) (2018), eaat8800.
[22] S. Brown, S. Kumar, B. Sharma, Intra-articular targeting of nanomaterials for the treatment of osteoarthritis, Acta Biomater. 93 (2019) 239–257.
[23] S. Brown, J. Pistiner, I.M. Adjei, B. Sharma, Nanoparticle properties for delivery to cartilage: the implications of disease state, synovial fluid, and off-target uptake, Mol. Pharm. 16 (2) (2019) 469–479.
[24] T.E. Kavanaugh, T.A. Werfel, H. Cho, K.A. Hasty, C.L. Duvall, Particle-based technologies for osteoarthritis detection and therapy, Drug Deliv Transl Res 6 (2) (2016) 132–147.

[25] M. Eugenia, M. Cruz, M.M. Gaspar, M.B.F. Martins, M.L. Corvo, Liposomal superoxide dismutases and their use in the treatment of experimental arthritis, Methods Enzymol. 391 (2005) 395–413.
[26] X. Yun, V.D. Maximov, J. Yu, H. Zhu, A.A. Vertegel, M.S. Kindy, Nanoparticles for targeted delivery of antioxidant enzymes to the brain after cerebral ischemia and reperfusion injury, J Cerebr Blood F Met 33 (4) (2013) 583–592.
[27] F.P. Chang, Y.P. Chen, C.Y. Mou, Intracellular implantation of enzymes in hollow silica nanospheres for protein therapy: cascade system of superoxide dismutase and catalase, Small 10 (22) (2014) 4785–4795.
[28] O. Onaca, D.W. Hughes, V. Balasubramanian, M. Grzelakowski, W. Meier, C. G. Palivan, SOD antioxidant nanoreactors: influence of block copolymer composition on the nanoreactor efficiency, Macromol. Biosci. 10 (5) (2010) 531–538.
[29] B. Katana, P. Rouster, G. Varga, S. Murath, K. Glinel, A.M. Jonas, I. Szilagyi, Self-assembly of protamine biomacromolecule on halloysite nanotubes for immobilization of superoxide dismutase enzyme, ACS Appl. Bio Mater. 3 (1) (2020) 522–530.
[30] P. Rouster, M. Pavlovic, I. Szilagyi, Immobilization of superoxide dismutase on polyelectrolyte-functionalized titania nanosheets, Chembiochem 19 (4) (2018) 404–410.
[31] G.D. Mao, M.J. Poznansky, Electron spin resonance study on the permeability of superoxide radicals in lipid bilayers and biological membranes, FEBS Lett. 305 (3) (1992) 233–236.
[32] J. Ghitman, E.I. Biru, R. Stan, H. Iovu, Review of hybrid PLGA nanoparticles: future of smart drug delivery and theranostics medicine, Mater. Des. 193 (2020) 108805.
[33] E. Sah, H. Sah, Recent trends in preparation of poly(lactide-co-glycolide) nanoparticles by mixing polymeric organic solution with antisolvent, J. Nanomater. 2015 (2015) 794601.
[34] E. Rideau, R. Dimova, P. Schwille, F.R. Wurm, K. Landfester, Liposomes and polymersomes: a comparative review towards cell mimicking, Chem. Soc. Rev. 47 (23) (2018) 8572–8610.
[35] D.E. Discher, A. Eisenberg, Polymer vesicles, Science 297 (5583) (2002) 967–973.
[36] P.J. Altshuler, A.R. Schiazza, L.J. Luo, M.R. Helmers, B. Chhay, J.S.J. Han, R. Hu, D.A. Herbst, A. Tsourkas, Z.L. Cheng, P. Atluri, Superoxide dismutase-loaded nanoparticles attenuate myocardial ischemia-reperfusion injury and protect against chronic adverse ventricular remodeling, Adv. Ther. 4 (6) (2021) 2100036.
[37] S. Kartha, L.S. Yan, C.L. Weisshaar, M.E. Ita, V.V. Shuvaev, V.R. Muzykantov, A. Tsourkas, B.A. Winkelstein, Z.L. Cheng, Superoxide dismutase-loaded porous polymersomes as highly efficient antioxidants for treating neuropathic pain, Adv Healthc Mater 6 (17) (2017) 1700500.
[38] J.M. McCord, I. Fridovich, Superoxide dismutase. An enzymic function for erythrocuprein (hemocuprein), J. Biol. Chem. 244 (22) (1969) 6049–6055.
[39] H. Jia, X. Ma, W. Tong, B. Doyran, Z. Sun, L. Wang, X. Zhang, Y. Zhou, F. Badar, A. Chandra, X.L. Lu, Y. Xia, L. Han, M. Enomoto-Iwamoto, L. Qin, EGFR signaling is critical for maintaining the superficial layer of articular cartilage and preventing osteoarthritis initiation, Proc. Natl. Acad. Sci. U. S. A. 113 (50) (2016) 14360–14365.
[40] I. Futami, M. Ishijima, H. Kaneko, K. Tsuji, N. Ichikawa-Tomikawa, R. Sadatsuki, T. Muneta, E. Arikawa-Hirasawa, I. Sekiya, K. Kaneko, Isolation and characterization of multipotential mesenchymal cells from the mouse synovium, PLoS One 7 (9) (2012), e45517.
[41] B. Carames, M. Olmer, W.B. Kiosses, M.K. Lotz, The relationship of autophagy defects to cartilage damage during joint aging in a mouse model, Arthritis Rheumatol. 67 (6) (2015) 1568–1576.
[42] H. Jia, X. Ma, Y. Wei, W. Tong, R.J. Tower, A. Chandra, L. Wang, Z. Sun, Z. Yang, F. Badar, K. Zhang, W.J. Tseng, I. Kramer, M. Kneissel, Y. Xia, X.S. Liu, J.H. C. Wang, L. Han, M. Enomoto-Iwamoto, L. Qin, Loading-induced reduction in sclerostin as a mechanism of subchondral bone plate sclerosis in mouse knee joints during late-stage osteoarthritis, Arthritis Rheumatol. 70 (2) (2018) 230–241.
[43] Y. Wei, L. Luo, T. Gui, F. Yu, L. Yan, L. Yao, L. Zhong, W. Yu, B. Han, J.M. Patel, J. F. Liu, F. Beier, L.S. Levin, C. Nelson, Z. Shao, L. Han, R.L. Mauck, A. Tsourkas, J. Ahn, Z. Cheng, L. Qin, Targeting cartilage EGFR pathway for osteoarthritis treatment, Sci. Transl. Med. 13 (576) (2021), eabb3946.
[44] A. Mathiessen, P.G. Conaghan, Synovitis in osteoarthritis: current understanding with therapeutic implications, Arthritis Res. Ther. 19 (1) (2017) 18.
[45] A.G. Bajpayee, C.R. Wong, M.G. Bawendi, E.H. Frank, A.J. Grodzinsky, Avidin as a model for charge driven transport into cartilage and drug delivery for treating early stage post-traumatic osteoarthritis, Biomaterials 35 (1) (2014) 538–549.
[46] Y.L. Wei, L.S. Yan, L.J. Luo, T. Gui, B. Jang, A. Amirshaghaghi, T.Y. You, A. Tsourkas, L. Qin, Z.L. Cheng, Phospholipase A(2) inhibitor-loaded micellar nanoparticles attenuate inflammation and mitigate osteoarthritis progression, Sci. Adv. 7 (15) (2021), eabe6374.
[47] R.F. Loeser, S.R. Goldring, C.R. Scanzello, M.B. Goldring, Osteoarthritis: a disease of the joint as an organ, Arthritis Rheum. 64 (6) (2012) 1697–1707.
[48] C.Y. Wenham, P.G. Conaghan, The role of synovitis in osteoarthritis, Ther. Adv. Musculoskelet. Dis. 2 (6) (2010) 349–359.
[49] X. Wang, D.J. Hunter, X. Jin, C. Ding, The importance of synovial inflammation in osteoarthritis: current evidence from imaging assessments and clinical trials, Osteoarthritis Cartilage 26 (2) (2018) 165–174.
[50] B. Bartok, G.S. Firestein, Fibroblast-like synoviocytes: key effector cells in rheumatoid arthritis, Immunol. Rev. 233 (1) (2010) 233–255.
[51] B.J.E. de Lange-Brokaar, A. Ioan-Facsinay, G.J.V.M. van Osch, A.M. Zuurmond, J. Schoones, R.E.M. Toes, T.W.J. Huizinga, M. Kloppenburg, Synovial inflammation, immune cells and their cytokines in osteoarthritis: a review, Osteoarthritis Cartilage 20 (12) (2012) 1484–1499.